Nuclear Physics B56 (1973) 15–45. North-Holland Publishing Company

# STRANGE PARTICLE PRODUCTION FROM $\pi^-$p INTERACTIONS AT 1.69 GeV/$c$†

D.W. THOMAS ‡‡, A. ENGLER, H.E. FISK ‡ and R.W. KRAEMER
*Carnegie-Mellon University, Pittsburgh, Pennsylvania 15213*

Received 4 January 1973

Abstract: The three-body final states $\Sigma^{\pm}\pi^{\mp}K^{0}$, $\Sigma^{0}\pi^{-}K^{+}$ and $\Lambda\pi^{0}K^{+}_{0}$ produced from $\pi$p interactions at 1.69 GeV/$c$ are examined. The quasi-two-body state $\Lambda(1405)K^{0}$ is discussed in detail. In particular, the spin of $\Lambda(1405)$ is determined, *via* the method of Byers and Fenster, to be consistent with $\frac{1}{2}$. The $\Sigma^{\pm}\pi^{\mp}$ mass spectrum is compared to that produced by various zero-range and effective-range parametrizations and the $\Lambda(1405)$ is found to have a mass of 1405 MeV and width of 45–55 MeV. Production and decay characteristics of the quasi-two-body states $\Sigma(1385)^{0}K^{+}_{0}$ are reported.

## 1. Introduction

In this paper experimental results are presented on strange-particle three-body final states resulting from $\pi^-$p interactions at 1.69 GeV/$c$. In particular, we report on the reactions

$$\pi^{-}p \to \Sigma^{\pm}\pi^{\mp}K^{0}, \tag{1}$$

$$\to \Sigma^{0}\pi^{0}K^{+}, \tag{2}$$

$$\to \Lambda\pi^{0}K^{+}_{0}. \tag{3}$$

The c.m. energy (2025 MeV/$c^2$) was chosen so as to be simultaneously at a point above threshold for the above reactions where the yield was known but below the $K^{*}(890)$ threshold. In this way we were able to isolate $\Sigma\pi$ and $\Lambda\pi$ states without the complications of competing $K\pi$ resonant states. Previously a Berkeley group [1] has published data on the same final states at this momentum as part of an exposure extending from 1.5 to 4.2 GeV/$c$. Their statistics at this energy were sparse; the present experiment represents a factor of six more data.

† Work supported by the US Atomic Energy Commission.
‡ Present address: Bell Telephone Laboratories, Holmdel, New Jersey.
‡‡ Present address: National Accelerator Laboratory, Batavia, Illinois 60510.

The primary purpose of the experiment was to attempt a determination of the $\Lambda(1405)$ spin-parity, using the method of Byers and Fenster [2] in a production reaction leading to a polarized $\Lambda(1405)$ sample. It has been pointed out [3] that even though the $\Lambda(1405)$ is believed to have $J^P = \frac{1}{2}^-$, little direct evidence has previously been available on the spin and no direct evidence existed on the parity. In this continuation of our previous work [4], we have been able to verify that $J = \frac{1}{2}$ is consistent with the data but are unable to make a parity determination because $\Lambda(1405)$ is produced unpolarized. The $\Sigma^{\pm}\pi^{\mp}$ mass spectrum is examined, however, and the shape compared to that predicted by the results of published zero-range and effective-range $K$-matrix parametrizations of low-energy $\bar{K}N$ data. We find this spectrum consistent only with a mass of approximately 1405 MeV and a width of 45–55 MeV and in strong disagreement with solutions yielding high mass and narrow width. Finally, $\Lambda\pi^0$ mass spectra and $\Sigma(1385)^0$ production properties are examined. Total and differential cross sections are presented as are those for the two-body states $\Lambda K$, $\Sigma^0 K^+$.

## 2. Experimental procedure

### *2.1. Exposures*

This experiment is based on data extracted from three exposures of $\pi^- p$ at 1.69 GeV/$c$ incident momentum. The initial exposure (E20) consisted of approximately 200k pictures in the BNL 20-inch hydrogen chamber. These data were taken in 1964 and partial results have been published [4]. Subsequent runs of 100k (E31a) and 200k (E31b) pictures in the BNL 31-inch hydrogen chamber were taken with the chamber situated in a medium-energy separated beam at the AGS and the negative pion beam has a nominal momentum spread, $\Delta p/p$, of 1% FWHM. The film was scanned for all strange-particle-production topologies. Since these events constitute less than 5% of the total cross section at 1.69 GeV/$c$, it was necessary to produce a reasonable level of discrimination at the scanning stage to keep the number of events to be measured within reasonable limits. Most strange-particle signatures can be found with high efficiency. However, the decay $\Sigma^+ \to p\pi^0$ is more subtle because of the small lab angle between the $\Sigma^+$ and proton. We, therefore, established broad scanning criteria so as to minimize detection losses. An acceptable topology included any of the following:

(a) A vee from a production vertex which has charged prongs.

(b) Two vees from a zero-prong (all neutral) production vertex. All events with zero prongs plus a single vee were rejected.

(c) A charged decay wherein the decaying track made a projected angle of 40° or less with the incident pion. The kinematic limit for the corresponding $\Sigma$ space angle was 32°.

Measurement failures were remeasured no more than twice and appropriate correc-

tions were made to the total cross sections (subsect. 2.3) for events which were finally deemed unmeasurable.

Events were measured in each of three views on a film plane digitizing machine. The measured track points were input to a standard version of the geometry program TVGP. Checks were made to ensure the values of the experiment-dependent input parameters were justified. Kinematic fitting was done with the program SQUAW. The fraction of pions in the beam was estimated from a study of randomly selected samples of E31. A fiducial region was scanned for total interactions, including completely neutral final states. In the same volume the total number of entering beam tracks was recorded. The process was repeated and the scan efficiency found to be 98%. The total number of interactions, corrected for efficiency was compared to the number expected from the $\pi^-$p total cross section at this energy of 34.2 mb [5]. The results are consistent with $(97^{+3}_{-6})$% pions if the remaining particles produce no strong interactions. Thus, there was an upper limit of 10% contamination in the beam and a correction of 5% was used in cross-section determination.

This experiment was not plagued by kinematic fitting ambiguities. Less than 1% of the events gave acceptable ($P(\chi^2) > 0.005$) fits to more than one final state hypothesis. Visual ionisation checks removed most ambiguities and events which remained ambiguous were few in number and were distributed according to highest chi-squared probability.

### 2.2. Systematic bias

We proceed now to a limited discussion of biases inherent in the experiment. A detailed discussion is also available [6].

Scanning losses can be grouped into two classes:

(a) random loss of easily visible events, and

(b) non-random loss biased against subtle configurations which can distort the final samples.

A rescan of the film will generally allow one to correct for loss (a). In this experiment, losses were found to be slightly topology dependent and efficiencies varied from 94 to 98%.

Corrections for losses (b) are not so easily made. An example of such a bias is as follows. Consider the decay process $A \to D + E$ in the lab frame. Events for which the normal to the decay plane is perpendicular to the optic ($Z$) axis could be difficult to detect because of the apparent collinearity of the track pairs ($A$, $D$), ($A$, $E$) or, in the case of $\Lambda^0$ or $K^0$, the pair ($D$, $E$). The loss of events would be apparent in a plot of the angle

$$\eta = \cos^{-1} \left| \frac{(\hat{A} \times \hat{Z})}{|\hat{A} \times \hat{Z}|} \cdot \frac{(\hat{A} \times \hat{D})}{|\hat{A} \times \hat{D}|} \right|$$

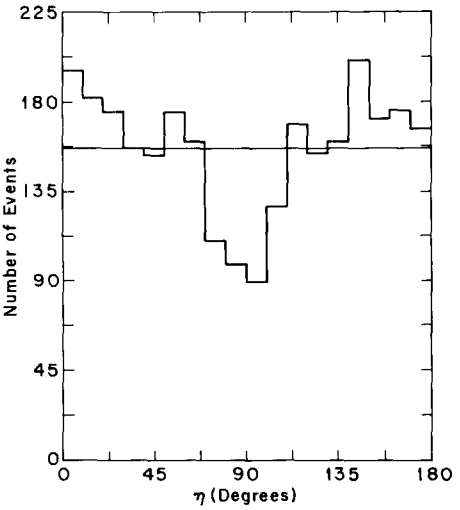


Fig. 1. Distribution of the angle $\eta$ (subsect. 2.2) for $\Sigma^-$ decay from the final state $\Sigma^- K^+$.

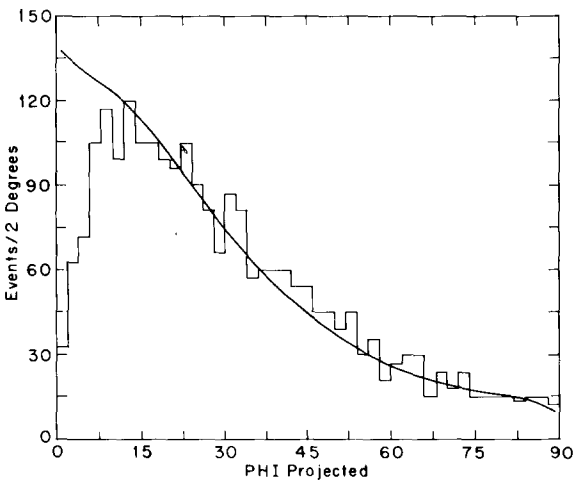


Fig. 2. Distribution in the projected angle $\phi$ for $\Sigma^-$ decay. The curve is the predicted distribution normalized for $\phi$ (projected) $> 20°$.

For no losses in the sample the distribution in $\eta$ must be isotropic. The distribution in $\eta$ is, in fact, isotropic for both $\Lambda^o$ and $K^o$ decay (not shown). The case for $\Sigma^-$ decay from the final state $\Sigma^- K^+$ is shown in fig. 1 where a definite bias is seen.

Because losses were more severe in $\Sigma^\pm$ decay than in either the $\Lambda$ or $K^o$ samples, a Monte-Carlo study, based on the $\Sigma^-$ momentum and isotropic decay distributions

for the final state $\Sigma^- K^+$, was undertaken to parameterize the expected distribution in the projected angle, $\phi$, between the projected $\Sigma$ track and the projected decay pion. Details of this study are also given in ref. [6]. The result is shown in fig. 2 where we show the predicted distribution in $\phi$ normalized to the data with $\phi > 20°$. From this graph a detection efficiency function was constructed and applied to all events having charged $\Sigma$ decays.

All decay data were constructed for short and long track length detection bias. The scanning efficiency was uniform for all decays between 4 mm projected length and the distance to the walls of the fiducial volume. Events outside this region were rejected and the remaining events weighted accordingly.

We were able to confirm our $\Sigma$ and $\Lambda$ correction procedures in the following ways:

(a) Biases in hyperon decay distributions for the states $\Sigma^- K^+$, $\Lambda^o K^o$ disappear.

(b) In the three-body final states $\Sigma^\pm \pi^\mp K^o$ and $\Lambda K^+ \pi^-$, the expected ratios of events with visible vee to without visible vee are satisfied.

(c) The ratio $\Sigma^+ \to p\pi^o / \Sigma^+ \to n\pi^+$ was $1.1 \pm 0.2$ for the three-body final states.

(d) The $\Sigma^-$, $\Sigma^+$, $\Lambda^o$, $K^o$ lifetimes were found to be in good agreement with the present world averages.

Finally, a Monte-Carlo study was undertaken to determine the effect of the weighting process on the quasi-two-body (resonant) states $\Sigma(1385)K$ and $\Lambda(1405)K$. We find

(a) the average weight as a function of $\Lambda\pi$ or $\Sigma\pi$ invariant mass or production $\cos\theta_{cm}$ is essentially constant.

(b) the weighting procedure did not affect the results of the moments analysis used in spin-parity determinations.

A sensitive test of bias in the measured chamber magnetic field can be made by determining the masses of $\Lambda^o$ and $K^o$. Use is made of the measured momenta of the two charged tracks and the invariant mass, $M$, is calculated. Since the mass depends directly upon the normalization of $H$, the latter was varied around the measured central value and the change in $M$ observed. For our final setting for $H$ (21.8 kG), Gaussian fits to the mass distributions gave the parameters (in MeV) $M(K^o) = 497.7$, $\sigma(K^o) = 6.4$, $M(\Lambda^o) = 1115.6$, $\sigma(\Lambda^o) = 2.1$.

### 2.3. Total cross section

The total cross section for a given reaction is given by $\sigma = N/(\rho L)$ where $N$ is the weighted† number of events found in a limited fiducial volume, $\rho$ is the target proton density, and $L$ is the total path length available for event production in the volume. A beam count was taken every 50 frames in a subsample of E31. The mean

† The data were corrected as follows: (a) scanning efficiency, 96%; (b) measurement efficiency, 92%; (c) geometric detection efficiency, 80% and (d) branching ratio to neutral channels. These corrections are topology dependent and only average values are quoted here.

Table 1
Final state total cross sections

| Final state | Fitted events | Weighted events | $\sigma(\mu b)$ | $\delta\sigma(\mu b)$ |
|---|---|---|---|---|
| $\Sigma^- K^+$ | 2014 | 2859 | 190.0 | 12.0 |
| $\Sigma^0 K^0$ | 255 | 403 [a] | 121.0 | 10.0 |
| $\Lambda K^0$ | 370 | 581 [a] | 174.0 | 14.0 |
| $\Sigma^- \pi^+ K^0$ | 284 | 378 | 25.1 | 2.2 |
| $\Sigma^+ \pi^- K^0$ $(\Sigma^+ \to p\pi^0)$ | 94 | 154 | 10.3 | 1.2 |
| $\Sigma^+ \pi^- K^0$ $(\Sigma^+ \to n\pi^+)$ | 110 | 148 | 9.9 | 1.2 |
| $\Sigma^- K^+ \pi^0$ | 148 | 207 | 13.8 | 1.4 |
| $\Sigma^0 K^+ \pi^-$ | 140 | 192 [a] | 19.1 | 1.9 |
| $\Lambda K^+ \pi^-$ | 560 | 762 [a] | 76.0 | 5.5 |
| $\Lambda K^0 \pi^0$ | 260 | 348 [a] | 104.0 | 8.0 |
| $K^0 \bar{K}^0 n$ | 12 | 14 [a] | 8.3 | 2.9 |
| $K^0 K^- p$ | 10 | 14 [a] | 2.9 | 0.9 |

[a] Does not include neutral branching ratio correction.

number of tracks per frame was 24.5 and the path length per track, corrected for curvature, attenuation by decay and interaction, and beam purity was 46.1 cm. This corresponds to a microbarn equivalent of 8.1 events per $\mu$b for the sample chosen. The microbarn equivalent of the total sample (E20 + E31), for an equal fiducial volume, was assumed to scale by the total number of strange particle events observed and the total cross section results are given in table 1. The results agree well with those at 1.69 GeV/$c$ of ref. [1]. Analyses of two and three-body final states presented in this paper are based, however, on a data sample taken from a fiducial region larger than that used for cross section determinations.

## 3. Three-body final states

### 3.1. $\Sigma^\pm \pi^\pm K^0$

#### 3.1.1. Interpretation of the $\Sigma\pi$ mass spectrum

The $\Lambda(1405)$ state decays with equal probability into $\Sigma^+\pi^-$, $\Sigma^-\pi^+$ and $\Sigma^0\pi^0$. We have observed each mode but have not analysed $\Sigma^0\pi^0$ because it constitutes an unconstrained fit. The $\Sigma\pi$ mass spectrum (unweighted) from $\Sigma^\pm\pi^\pm K^0$ is shown in fig. 3. The total sample is 651 events with 470 events lying between $\Sigma\pi$ threshold ($\sim$ 1332 MeV) and $\bar{K}N$ threshold ($\sim$ 1430 MeV). Since, however, these events contain a contribution from the production and decay of $\Sigma(1385)^0$, one must be convinced the signal is not dominated by that state. We can make the following statements concerning the $\Sigma\pi$ mass spectrum:

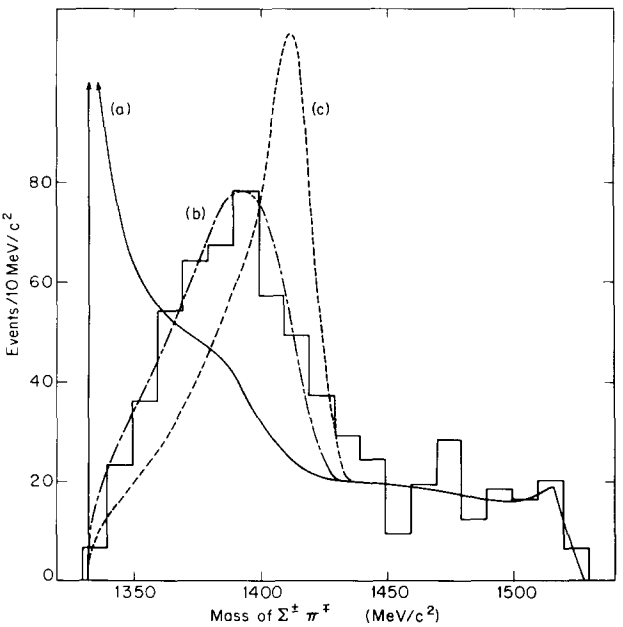


Fig. 3. Mass distribution of $\Sigma^{\pm}\pi^{\mp}$. The curves are the normalized distributions predicted by the parameters of (a) Berley et al. [18], (b) Kim [13] and (c) Martin and Sakitt [19].

(a) From our analysis of the state $\Lambda^0\pi^0K^0$ (subsect. 3.2) and from the measured branching fraction of $\Sigma(1385) \to \Sigma\pi$, we expect no more than 50 ± 10 events due to $\Sigma(1385)^0$ production to lie in the 1340 – 1440 MeV mass region.

(b) Examination of the production angular distributions for $\Sigma(1385) \to \Lambda^0\pi^0$ (fig. 8) and for the $\Sigma^{\pm}\pi^{\pm}$ events in the peak region of fig. 3, shows them to be quite dissimilar. The $\Lambda^0\pi^0$ events are peaked at 90° in the c.m.s. while the $\Sigma\pi$ events (fig. 5) show forward production.

(c) In a spin-parity analysis (subsect. 3.1.2), using the Byers-Fenster [2] technique we show the $\Sigma(1385)^0$ is produced with a spin moment $t_2^0 = 0.32 \pm 0.06$. It is this large moment which allows one to exclude $J = \frac{1}{2}$ for this state and which also produces a non-isotropic decay angular distribution (subsect. 3.2). Application of the same technique to the $\Sigma\pi$ data yield a moment $t_2^0 = 0.05 \pm 0.06$ and an isotropic decay angular distribution consistent with $J = \frac{1}{2}$.

(d) The absence of interference with background or another resonant state requires the distribution in $\hat{\boldsymbol{\Sigma}} \cdot \hat{\boldsymbol{Y}}^*$, in the $Y^*$ rest frame to be symmetric (and isotropic for $J = \frac{1}{2}$). For the $\Sigma^{\pm}\pi^{\mp}$ events, this distribution is isotropic and has a forward/backward ratio of 1.03 ± 0.10.

Thus, the $\Sigma^{\pm}\pi^{\mp}$ data indicate the production of a state different from $\Sigma(1385)$ and suggest this state does not interfere strongly with any other.

Alternate interpretations of the nature of $\Sigma(1405)$ have been proposed:

(a) as an S-wave virtual bound state of the $\bar{K}N$ system [7], and

(b) as an isoscalar unitary singlet member of an SU(6)–$L$ supermultiplet [8].

Dalitz [9] has pointed out the two interpretations are in opposition. The supermultiplet model requires the $\Lambda(1405)$ to exist because of strong forces which give rise to the complete multiplet and not because of particular forces which are important only for $\Lambda(1405)$. Alternately, in the analysis of multichannel $\bar{K}N$ scattering $\Lambda(1405)$ is identified with a pole in the reduced matrix generated by its connection with the closed $\bar{K}N$ channel. Regardless which of (a) or (b) is correct, the experimental facts are that the parity of $\Lambda(1405)$ has not yet been determined in a production experiment whereas the spin has been shown to be consistent with $\frac{1}{2}$ (ref. [4] and subsect. 3.1.2 of this paper).

Extensive analyses of $\bar{K}N$ scattering data have been completed and the results are available in the literature [10]. Techniques used are the constant scattering length (CSL), the zero-range $K$-matrix (ZRA), and the effective-range $K$-matrix (ERA) parametrizations. All formalisms allow smooth extrapolation to below $\bar{K}N$ threshold where it is also important to observe the behaviour of the partial-wave amplitudes. In particular, the $S_{01}$ amplitude in the $\Sigma\pi$ channel is crucial to the description of $\Lambda(1405)$. Regardless of parametrization, a common result is the prediction of an $I = 0$ S-wave bound state of the $\bar{K}N$ system.

Recently, however, Bunnel et al. [11] and Cline et al. [12] have studied the $\Lambda\pi$ and $\Sigma\pi$ final states produced in $K^-d$ interactions. Invoking the impulse approximation they observe $\bar{K}N \to \Lambda\pi, \Sigma\pi$ below the $\bar{K}N$ threshold. Their analyses indicate the $\Lambda(1405)$ is not strongly coupled to $\bar{K}N$ and $\Sigma(1385)$ production is larger than that predicted by the ERA analysis of Kim [13]. For the $\Sigma\pi$ final states, Cline et al. show the $S_{01}$ amplitude to be a repilsive background always lying in the second quadrant of the complex $T$ plane.

We have used both the ZRA and ERA models to fit the $\Sigma\pi$ mass spectrum. In the ZRA model [7], one defines a real, symmetric $K$ matrix

$$K_o \equiv \begin{bmatrix} K_{11} & K_{12} \\ K_{21} & K_{22} \end{bmatrix} \equiv \begin{matrix} \begin{bmatrix} \alpha & \beta \\ \beta & \gamma \end{bmatrix} \begin{matrix} \bar{K}N \\ \Sigma\pi \end{matrix} \\ \bar{K}N \quad \Sigma\pi \end{matrix}$$

where the zero subscript refers to isotropic spin. The S-wave transition matrix $T$ is related to the $K$ matrix through

$$T^{-1} = K^{-1} - iQ$$

where $Q$ is a diagonal matrix of channel momenta. Calling $q_1$ the $\bar{K}N$ relative momentum and $q_2$ the relative $\Sigma\pi$ momentum, it follows that

$$T_{22} = \frac{A}{1 - iq_2 A}$$

where

$$A = \gamma + \frac{iq_1\beta^2}{1 - iq_1\alpha} = \gamma - \frac{|q_1|\beta^2}{1 + \alpha|q_1|}$$

below the $\bar{K}N$ threshold. The cross section $\sigma(\Sigma\pi \to \Sigma\pi)$ is proportional to $|T_{22}|^2$ and the $\Sigma\pi$ mass spectrum, according to Watson's Theorem [14], is proportional to $q_2|T_{22}|^2$.

In the ERA model [15], the $K$ matrix is related to a matrix $M$ through

$$M = Q^{l+\frac{1}{2}} K^{-1} Q^{l+\frac{1}{2}},$$

where $Q^{l+\frac{1}{2}}$ is again a diagonal matrix of channel momenta and $l$ is the relative orbital angular momentum. Then, in the notation of Ross and Shaw, one has

$$T = K(1 - iK)^{-1} = Q^{l+\frac{1}{2}} (M - iQ^{2l+1})^{-1} Q^{l+\frac{1}{2}}.$$

Finally, $M$ is expanded about some reference energy, $E_0$, which is commonly taken to be the $\bar{K}N$ threshold:

$$M(E) = M(E_0) + \tfrac{1}{2}R(Q^2(E) - Q^2(E_0)).$$

$R$ is a diagonal matrix of effective ranges and the above expansion of $M(E)$ is for S-waves only. Thus, $T$ is parametrized in terms of five $I = 0$ real numbers: $M_{11}(E_0)$, $M_{22}(E_0)$, $M_{12}(E_0)$, $R_1$ and $R_2$.

Elastic scattering in the $\Sigma\pi$ channel is given by the amplitude

$$T_{22} = \frac{q_2(M_{11} + |q_1|)}{(M_{11} + |q_1|)(M_{22} - iq_2) - M_{12}^2}$$

below $\bar{K}N$ threshold. The $\Sigma\pi$ scattering cross section is proportional to $|T_{22}|^2/q_2^2$ and the $\Sigma\pi$ mass spectrum to $|T_{22}|^2/q_2$. To describe the observed $\Sigma\pi$ mass spectrum we have added incoherent contributions from Lorentz-invariant phase space, $\Sigma(1385)$, $\Lambda(1520)$ and $\Lambda(1405)$. Normalization to the phase space background is fixed in the mass region 1440–1495 MeV and amounts to 43% of the total. The $\Sigma(1385)$ and $\Lambda(1520)$ contributions are 8% and 3%; the former was discussed previously in this Section. The remaining 46% of the intensity is attributed to $\Lambda(1405)$. Input parameters for the ZRA and ERA models for $\Lambda(1405)$ were taken from the literature. Thus, there are no free parameters in the description of the $\Sigma\pi$ intensity and $\chi^2$ was calculated for each set of input parameters. We have summarized our results for the $\Sigma\pi$ mass spectrum in table 2 and the following statements can be made:

(a) The data are inconsistent with any ZRA parameters previously published. In general, these solutions predict a higher mass ($> 1415$ MeV) and a narrower width

Table 2
Results of fitting the $\Sigma^{\pm}\pi^{\mp}$ mass spectrum using ZRA and ERA parameters [$\alpha$, $\beta$, $\gamma$, $R_1$, and $R_2$ are given in fm; $M_{11}$, $M_{12}$, and $M_{22}$ are given in $(\text{fm})^{-1}$; the number of degrees of freedom is 15]

ZRA parameters

| Ref. | $\alpha$ | $\beta$ | $\gamma$ | $\chi^2$ | $P(\chi^2)$ |
|---|---|---|---|---|---|
| [19] | − 1.88 | − 0.92 | − 0.36 | 128. | $< 10^{-5}$ |
| [20] | − 2.40 | − 1.21 | − 1.05 | 450. | $< 10^{-5}$ |
| [18] | − 2.04 | − 1.28 | − 0.40 | 36.4 | 0.002 |
| [17] | − 1.68 | − 0.86 | − 0.09 | 42.0 | 0.00025 |

ERA parameters

| Ref. | $M_{11}(E_0)$ | $M_{12}(E_0)$ | $M_{22}(E_0)$ | $R_1$ | $R_2$ | $\chi^2$ | $P(\chi^2)$ |
|---|---|---|---|---|---|---|---|
| [13] | 0.00 | − 1.11 | 2.04 | 0.54 | − 0.89 | 18.4 | 0.25 |
| [13] a) | 0.00 | − 1.11 | 2.04 | 0.0 | 0.0 | 27.1 | 0.03 |
| [18] | 0.03 | − 1.50 | 2.61 | 0.23 | 1.30 | 320.0 | $< 10^{-5}$ |
| [17] | 0.03 | − 1.09 | 1.89 | − 0.38 | 0.61 | 25.6 | 0.045 |

a) Kim's solution [13] with $R_{1,2}$ set to zero by us.

(< 35 MeV) than we observe. However, a successful ZRA fit to the world $\bar{K}N$ above threshold data along with our $\Sigma\pi$ mass spectrum has been attained and is reported in the following paper [16].

(b) The ERA parameters of Kim [13] and of Thompson [17] reproduce the shape of the mass spectrum well. The mass and width quoted by Kim are $M = 1403 \pm 3$, $\Gamma = 50 \pm 5$ MeV. Thompson's parameters yield $M = 1408$, $\Gamma = 45$ MeV where, since the mass spectrum is not symmetric, we have taken the width to be defined by the $\Sigma\pi$ phase shifts at 45 and 135 degrees. Thus, in the context of this rather unsophisticated model for the $\Sigma\pi$ mass spectrum, the data are consistent only with a $\Lambda(1405)$ mass of approximately 1405 and a width of 45–55 MeV. The ERA parameters of Berley et al. [18] reproduce the data poorly but this is not surprising since their fit was made to data in the limited momentum range 350 to 430 MeV/c. In fig. 3 we show the $\Sigma\pi$ mass distribution predicted by some ZRA and ERA parameters in the framework of the model described above.

*3.1.2. Spin-parity of Λ(1405)*

Byers and Fenster [2] have developed a general method of determining the spin and parity of a resonance, $Y^*$, through the decay sequence:

$Y^* \to Y + \pi$ (strong decay; spin $J \to$ spin $\frac{1}{2}$ + spin 0),

$Y \to N + \pi$ (parity violating decay providing information on the polarization of the $Y^*$).

The spin state population of the $Y^*$ may be expressed in terms of multipole moments $t_L^M (0 \leqslant L \leqslant 2J)$, which are the expectation values of the irreducible tensors

$T_L^M$, of rank $L$, defined in the spin space of the Y*. The $T_L^M$ obey the same transformation laws under a spatial rotation as the spherical harmonics $Y_L^M$ and are formed from the expectation values of the spin operators **S** in the same way as the spherical harmonics are formed from the unit vector. Thus they have the property $T_L^{-M} = (-1)^M T_L^{M\dagger}$. The density matrix of the Y* may be expressed as

$$\rho = (2J+1)^{-1} \sum_{L,M} (2L+1)\, T_L^M\, t_L^{M*}$$

subject to the normalization condition

$$\mathrm{Tr}(T_{L'}^{M'}\, T_L^{M\dagger}) = \left(\frac{2J+1}{2L+1}\right) \delta_{LL'} \delta_{MM'} ,$$

which leads immediately to

$$t_L^M = \mathrm{Tr}\,(\rho\, T_L^M) .$$

The decay of the Y*, which can occur through orbital angular momentum states $L = J \pm \frac{1}{2}$ depending on the parity of the Y*, is described by the normalized angular distribution function $I(\theta, \phi)\mathrm{d}\Omega$ which is equal to the fraction of decay particles, Y, which occur in solid angle $\mathrm{d}\Omega$. Byers and Fenster have shown that this function is related to the multipole moments $t_L^M$ by

$$\eta_{L0}\, t_L^M = \langle Y_L^M \rangle = \int I(\theta, \phi)\, Y_L^M(\theta, \phi)\mathrm{d}\Omega$$

for even $L$, where $\eta_{L0}$ is related to a Clebsch-Gordan coefficient and $\theta$ and $\phi$ are the polar and aximuthal angles of the Y in the Y* rest frame.

As a consequence of parity conservation in the production process, the angular distribution function is related only to moments of even $L$. However, this relation does indeed provide a constraint on the spin of the Y* since $t_L^M = 0$ for $L > 2J$. Thus, the largest $L$ for which $t_L^M$ is non-zero sets a lower limit on $J$.

Moreover, if the spin states of the Y* are populated such that $t_L^M \neq 0$ for odd $L$, the parity of the resonance can be obtained by comparison of the longitudinal and transverse polarization of the Y, as a function of the Y* decay angle. The longitudinal Y polarization, defined by $(\hat{\mathbf{P}} \cdot \hat{\mathbf{k}})\hat{\mathbf{k}}$ where $\hat{\mathbf{k}}$ is a unit vector in the direction of the Y and **P** is the polarisation, is related to the multipole moments by

$$\eta_{L0}\, t_L^M = \int I(\theta, \phi)\, (\mathbf{P} \cdot \hat{\mathbf{k}})\, Y_L^M(\theta, \phi)\mathrm{d}\Omega$$

for odd $L$. The transverse polarization is related to $\gamma t_L^M$ where $\gamma$ is defined in terms of the two possible Y* decay amplitudes:

$$\gamma = (|A(J-\tfrac{1}{2})|^2 - |A(J+\tfrac{1}{2})|^2)/(|A(J-\tfrac{1}{2}|^2 + |A(J+\tfrac{1}{2})|^2) .$$

Thus the ratio of transverse to longitudinal polarization determines the $Y^*$ parity.

The expressions for $t_L^M$ and $\gamma t_L^M$ are complex. The real and imaginary parts are obtained from separate sums. We represent all of these sums in general by

$$\bar{S}^J = \frac{1}{N} \sum_i S_i^J$$

where the sum is over all $N$ events. The correlated variance matrix for these sums is

$$V_{JK} = \sum_i (S_i^J - \bar{S}^J)(S_i^K - \bar{S}^K)/N^2$$

The standard deviation in $S^J$ is then $\delta S^J = \sqrt{V_{jj}}$. Moreover, the variance matrix may be used to construct a chi-squared:

$$\chi^2 = \sum_{J,K} (S^J - S^{J*}) V_{JK}^{-1} (S^K - S^{K*})$$

where the $S^{J*}$ are the value expected under the hypothesis being tested.

For spin analysis alone, one determines the smallest $L'$ such that $t_L^M$ is consistent with zero for $L > L'$. Then the relation $t_L^M = 0$ for $L > 2J$, where $J$ is the spin of the particle, $Y^*$, sets a lower limit on $J$. A chi-squared is constructed based on the real and imaginary parts of all moments (with $M$ even), with $L > L'$. This is accomplished by setting $S^{J*} = 0$ for all sums which correspond to $L > L'$ and $S^{J*} = S^J$ for the remaining sums. For spin-parity analysis, only the odd-$L$ moments are used. In this case, the sums correspond to a comparison of the contribution of each event to the moments $t_L^M$ and $\gamma t_L^M$. If $s_i^J$ represents the contribution of event $i$ to one of the $t_L^M$ and $s_i^{J'}$, is the contribution to the corresponding $\gamma t_L^M$, the chi-squared function is based on the sums

$$S_+^J = \sum_i (s_i^J + s_i^{J'})/N\,, \qquad S_-^J = \sum_i (s_i^J - s_i^{J'})/N\,.$$

Each sum is tested for consistency with zero. The chi-squared function may be calculated for different $J$ and the number of terms (degrees of freedom) increases with $J$. However, since $\gamma = \pm 1$ for strong decays, one or both of these chi-squared confidence levels should be acceptable. If all moments are consistent with zero, both values of $\gamma$ are acceptable and no parity discrimination is possible.

Determination of the $\Lambda(1405)$ spin is based on 464 unweighted event from the final states $\Sigma^\pm \pi^\mp K^0$ with $\Sigma\pi$ invariant mass between 1360 and 1440 MeV. The moments $t_L^M$ obtained from the $\Lambda(1405)$ decay angular distribution (even $L$) and from longitudinal polarization (odd $L$) are listed in table 3 for $J \leqslant \frac{5}{2}$. All moments are consistent with zero. The spin analysis has also been done independently for different production and $\Sigma\pi$ mass selection criteria to minimize the possibility of cancel-

Table 3
Spin-parity moments for $\Lambda(1405)$

Spin analysis

| $J$ | $t_L^M$ | Re $t_L^M$ | $\delta$(Re $t_L^M$) | Im $t_L^M$ | $\delta$(Im $t_L^M$) |
|---|---|---|---|---|---|
| $\frac{1}{2}$ | $t_1^0$ | 0.07 | 0.08 | | |
| $\frac{3}{2}$ | $t_1^0$ | 0.15 | 0.19 | | |
| | $t_2^{-2}$ | 0.02 | 0.03 | − 0.03 | 0.03 |
| | $t_2^0$ | − 0.07 | 0.05 | | |
| | $t_3^{-2}$ | − 0.01 | 0.05 | 0.07 | 0.04 |
| | $t_3^0$ | − 0.06 | 0.06 | | |
| $\frac{5}{2}$ | $t_1^0$ | 0.23 | 0.28 | | |
| | $t_2^{-2}$ | 0.02 | 0.03 | − 0.03 | 0.03 |
| | $t_2^0$ | − 0.07 | 0.04 | | |
| | $t_3^{-2}$ | − 0.03 | 0.08 | 0.12 | 0.08 |
| | $t_3^0$ | − 0.10 | 0.11 | | |
| | $t_4^{-4}$ | 0.04 | 0.03 | 0.01 | 0.03 |
| | $t_4^{-2}$ | 0.04 | 0.04 | − 0.01 | 0.03 |
| | $t_4^0$ | 0.07 | 0.05 | | |
| | $t_5^{-4}$ | − 0.03 | 0.04 | 0.01 | 0.04 |
| | $t_5^{-2}$ | − 0.06 | 0.04 | − 0.03 | 0.04 |
| | $t_5^0$ | − 0.02 | 0.05 | | |

Parity analysis

| $J$ | $t_L^M$ | Re $t_L^M$ | $\delta$(Re $t_L^M$) |
|---|---|---|---|
| $\frac{1}{2}$ | $t_1^0$ | − 0.02 | 0.10 |
| | $\gamma t_1^0$ | 0.15 | 0.12 |

lation among average moments in different samples. The results of chi-squared tests for various cuts are summarized in table 4a. The distribution of $\cos\beta$ for the decay $\Lambda(1405) \to \Sigma\pi$, where $\beta$ is the angle between $\hat{\boldsymbol{\pi}}$ and the production normal in the $\Lambda(1405)$ rest frame, is shown in fig. 4. This distribution is symmetric and isotropic; both conditions are consistent with the decay of a $J = \frac{1}{2}$ state free from interference with other amplitudes. Thus, there is nothing in the data to suggest that $\Lambda(1405)$ is not a $J = \frac{1}{2}$ state.

The parity analysis of $\Lambda(1405)$ is based on 94 events having the decay $\Sigma^+ \to p\pi^0$.

Table 4a
Results of $\Lambda(1405)$ spin analysis for various selection criteria

| Selection criteria | No. of events | $\chi^2$ | $P(\chi^2)$ [a] |
|---|---|---|---|
| Total sample | 464 | 8.7 | 0.38 |
| $M(\Sigma\pi) < 1390$ MeV | 243 | 10.1 | 0.25 |
| $M(\Sigma\pi) > 1390$ MeV | 221 | 8.8 | 0.36 |
| $\hat{\pi} \cdot \hat{K} > 0.5$ [b] | 203 | 5.2 | 0.73 |
| $0.5 > \hat{\pi} \cdot \hat{K} > 0$ | 74 | 13.4 | 0.10 |
| $-0.5 < \hat{\pi} \cdot \hat{K} < 0$ | 103 | 13.1 | 0.11 |
| $-1.0 < \hat{\pi} \cdot \hat{K} < -0.5$ | 84 | 12.6 | 0.13 |

a) Confidence level for the joint probability that $J \neq \frac{3}{2}$ and $J \neq \frac{5}{2}$. 8 degrees of freedom.
b) $\hat{\pi}$ and $\hat{K}$ are unit vectors of the incoming pion and outgoing kaon in the production c.m.s.

Table 4b
Result of $\Lambda(1405)$ parity analysis assuming $J = \frac{1}{2}$

| No. of events | Hypothesis | Degrees of freedom | $\chi^2$ | $P(\chi^2)$ |
|---|---|---|---|---|
| 94 | $J^P = \frac{1}{2}^+$ | 1 | 0.33 | 0.58 |
| 94 | $J^P = \frac{1}{2}^-$ | 1 | 0.62 | 0.44 |

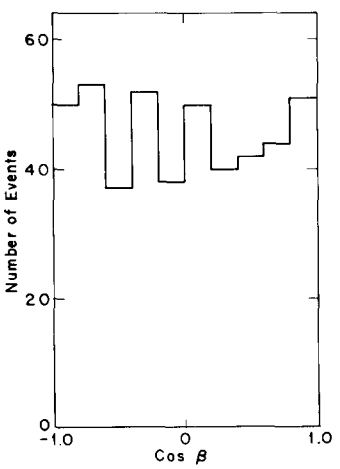


Fig. 4. Distribution of cos $\beta$ for the decay $\Lambda(1405) \rightarrow \Sigma\pi$ where $\beta$ is the angle between $\hat{\pi}$ and the production normal in the $\Lambda(1405)$ rest frame.

The analyzing power of this sample is high since $\alpha_0 = -0.96$. A parity determination for a $J = \frac{1}{2}$ state, however, depends on a non-zero moment $t_1^0$ since $t_1^0 = P/\sqrt{3}$ (for $J = \frac{1}{2}$), where $P$ is the magnitude of the $\Lambda(1405)$ polarization. Absence of significant polarization precludes a direct parity determination. In table 3 we also give $t_1^0$ and $\gamma t_1^0$ for the 94 event sample. Both are consistent with zero. Thus, no $\Lambda(1405)$ parity determination is possible and this is reflected in the acceptable confidence levels for either parity hypothesis given in table 4b.

*3.1.3. $\Lambda(1405)$ production angular distribution*

The production angular distribution† for the weighted $\Sigma^{\pm}\pi^{\mp}$ events lying between 1340 and 1430 MeV is shown in fig. 5. A Legendre polynomial fit to form

$$\frac{d\sigma}{d\Omega}(\mu b/sr) = \sum_n A_n P_n(\cos\theta) \tag{4}$$

is also shown and the coefficients, $A_n$, are given in table 5. Normalization is such that the total cross section for $\pi^- p \to \Lambda(1405)\, K^o$ is 46% of the cross section for $\pi^- p \to \Sigma^{\pm}\pi^{\mp}K^o$, no background subtraction has been made, and $A_0$ is normalized to $\sigma/4\pi$.

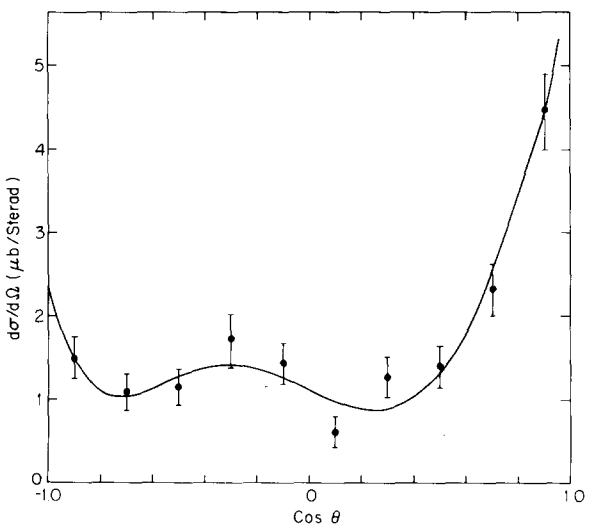


Fig. 5. Differential cross section for $\pi^- p \to \Lambda(1405) K^o$. The coefficients for the curve are given in table 5.

† The c.m. production angle convention used throughout is as follows: $\cos\theta = \hat{\mathbf{q}} \cdot \hat{\mathbf{q}}^1$ where the unit vectors $\hat{\mathbf{q}}$ and $\hat{\mathbf{q}}^1$ define the directions of the incoming proton and outgoing hyperon, respectively.

Table 5
Differential cross section and polarization expansion coefficients in μb/sr

| Final state | $\chi^2$ | Degrees of freedom | $P(\chi^2)$ | $A_0$ | $A_1$ | $A_2$ | $A_3$ | $A_4$ | $A_5$ | $A_6$ |
|---|---|---|---|---|---|---|---|---|---|---|
| $\Lambda(1405)K^0$ | 9.7 | 4 | 0.05 | 1.64 ± 0.08 | 1.02 ± 0.17 | 1.54 ± 0.23 | 0.96 ± 0.28 | 0.55 ± 0.28 | − 0.56 ± 0.36 | |
| $\Sigma(1385)^-K^+$ | 9.1 | 5 | 0.10 | 5.2 ± 0.5 | − 2.2 ± 0.4 | 1.0 ± 0.6 | 0.8 ± 0.5 | 1.0 ± 0.9 | | |
| $\Sigma(1385)^0K^0$ | 3.5 | 7 | 0.82 | 6.1 ± 0.8 | 1.2 ± 0.6 | − 5.2 ± 0.8 | | | | |
| $\Lambda K^0$ | 2.1 | 5 | 0.83 | 13.9 ± 1.2 | 9.8 ± 1.7 | 20.1 ± 2.6 | − 1.3 ± 2.2 | 12.8 ± 2.6 | | |
| $\Sigma^-K^+$ | 3.2 | 6 | 0.78 | 15.1 ± 1.0 | − 18.8 ± 1.2 | 4.1 ± 0.8 | 2.9 ± 0.7 | | | |
| $\Sigma^0K^0$ | 3.2 | 3 | 0.36 | 9.6 ± 0.8 | 5.3 ± 1.2 | 8.0 ± 1.5 | 16.2 ± 2.1 | 6.7 ± 2.5 | 10.4 ± 2.5 | 8.0 ± 3.3 |

| | | | | $B_1$ | $B_2$ | $B_3$ |
|---|---|---|---|---|---|---|
| $\Lambda^0K^0$ | 1.5 | 2 | 0.48 | −0.38 ± 0.22 | 0.26 ± 0.11 | 0.37 ± 0.13 |

### 3.2. The final states $\Lambda^0\pi^0 K^+_0$

#### 3.2.1. Mass and width of $\Sigma(1385)^0$

The $\Lambda\pi$ mass spectra for the final states $\Lambda^0\pi^- K^+$ (722 events unweighted) and $\Lambda^0\pi^0 K^0$ (330 events unweighted) are shown in figs. 6 and 7. Background is small in each case and the Dalitz plots (not shown) indicate $K^*(890)$ production is negligible. The maximum $K\pi$ mass attainable is 910 MeV; thus these reactions are well-suited for mass and width determinations. We now discuss the method, identical for both $\Lambda\pi^-$ and $\Lambda\pi^0$, used to extract these parameters.

Resonances production ($\Sigma(1385)$ and $K^*(890)$) was represented by Breit-Wigner functions having fixed mass, width and appropriate angular momentum barrier terms. The resonance processes and Lorentz-invariant phase space background were taken to add incoherently and the relative amount of each was determined from a maximum likelihood fit. The results are shown in table 6a. Next, the $\Lambda\pi$ mass resolution was determined by constructing an ideogram of effective mass errors propagated from the kinematics fitting program SQUAW. This resolution was found to be independent of $\Lambda\pi$ mass and to be adequately parametrized by a Gaussian of variance 1.7 MeV for $\Lambda\pi^-$ and 4.0 MeV for $\Lambda\pi^0$. Each $\Lambda\pi$ mass spectrum was then refitted, with background held fixed, to the same incoherent sum of phase space and Breit-Wigner functions with a Gaussian resolution function unfolded and mass and width as parameters. The maximum likelihood solutions are given in table 6b. For each state the mass and width parameters are essentially uncorrelated and the

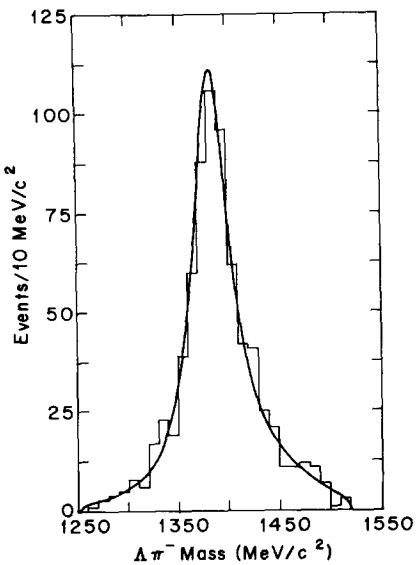


Fig. 6. $\Lambda\pi^-$ mass distribution from the final state $\Lambda\pi^- K^+$. The fitted curve is discussed in subsect. 3.2.1.

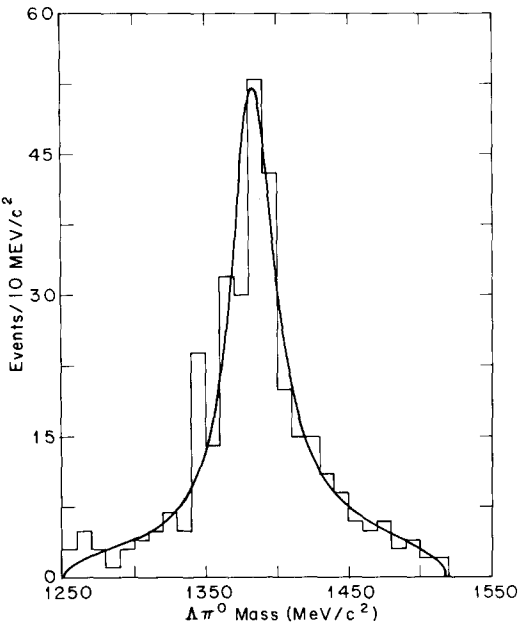


Fig. 7. $\Lambda\pi^0$ mass distribution from the final state $\Lambda\pi^0 K^0$. The fitted curve is discussed in subsect. 3.2.1.

Table 6a
Percentage contributions to the final states $\Lambda\pi^{\overline{0}}\ K^{+}_{0}$

| Final state | No. of events (unweighted) | Contribution (%) | Production state |
|---|---|---|---|
| $\Lambda\pi^- K^+$ | 722 | 87 ± 5 | $\Sigma(1385)^- K^+$ |
| | | 5 ± 3 | $\Lambda K^*(890)$ |
| | | 8 ± 6 | phase space |
| $\Lambda\pi^0 K^0$ | 330 | 73 ± 7 | $\Sigma(1385)^0 K^0$ |
| | | 2 ± 2 | $\Lambda K^*(890)$ |
| | | 15 ± 8 | phase space |

Table 6b
Mass and width parameters (MeV) for $\Sigma(1385)^{\overline{0}}$

| State | Mass | Width | ⟨Mass⟩ world | ⟨Width⟩ world |
|---|---|---|---|---|
| $\Sigma(1385)^-$ | 1387.1 ± 1.3 | 48.2 ± 4.0 | 1385.9 ± 1.5 | 36.3 ± 6.3 |
| $\Sigma(1385)^0$ | 1385.1 ± 2.0 | 39.3 ± 6.1 | | |

width parameter changed by less than 2 MeV with the inclusion of the resolution dependent terms. Finally, curves constructed from the best fit parameters are superimposed on the data of figs. 6 and 7.

Our results for $\Sigma(1385)^-$ are consistent with the present world averages published by the Particle Data Group [21]. However, no world average is given for the mass of width of $\Sigma(1385)^0$, presumably because of uncertain systematics or poor data quality. The present experiment yields measurements of the mass and width of $\Sigma(1385)^0$ from a final state which (a) has a constrained fit, (b) is isolated from competing production processes, and (c) has well understood resolution.

Mass splitting, within the SU(3) decuplet, due to electromagnetic and symmetry breaking strong interactions, has been calculated under specific assumptions [22]. In particular, the following are predicted:

$$\Delta^- - \Delta^0 = \Sigma^- - \Sigma^0 = \Xi^- - \Xi^0, \qquad \Delta^0 - \Delta^+ = \Sigma^0 - \Sigma^+,$$

where $\Delta$, $\Sigma$, $\Xi$ represents the masses of $\Delta(1236)$, $\Sigma(1385)$, and $\Xi(1529)$ in the appropriate charge state. From this experiment we obtain $\Sigma^- - \Sigma^0 = 2.0 \pm 2.4$ MeV and the Particle Data Group compilation gives $\Xi^- - \Xi^0 = 4.0 \pm 2.2$ MeV.

The mass difference $\Delta^- - \Delta^0$ is not available for comparison. However, making use of the world average of $1382.7 \pm 0.7$ MeV for $\Sigma(1385)^+$ and this experiment for the mass of $\Sigma(1385)^0$, we obtain $\Sigma^0 - \Sigma^+ = 2.4 \pm 2.1$ MeV.

### 3.2.2. *Spin-parity of $\Sigma(1385)$*

The spin-parity of $\Sigma(1385)$ has been determined to be $\frac{3}{2}^+$ by Shafer and Huwe [23] using the moments technique of Byers and Fenster. Since the present experiment yields $\Lambda\pi^0$ mass spectra with small background and no competing resonance production. we seek here to verify that $\frac{3}{2}^+$ is in agreement with the data and to determine the levels at which other spin-parities are rejected.

The analysis of $\Sigma(1385)^-$ is based on 553 unweighted events with $\Lambda\pi$ mass between 1360 and 1440 MeV. The moments, $t_L^M$, up to $J = \frac{5}{2}$ for these events are presented in table 7. The need for $J > \frac{1}{2}$ is clear. We have also analyzed the data as a function of $\Sigma(1385)^-$ production angle and find the moments depend strongly on production angle and the odd $L$ moments generally indicate the presence of polarization. The spin-parity confidence levels for the total sample and for the 276 events having $|\hat{\boldsymbol{\pi}}_{\text{in}}^- \cdot \hat{\mathbf{K}}_{\text{out}}^+| < 0.5$ are summarized in table 8. On the basis of the total sample it is possible to reject $J^P = \frac{1}{2}^{\pm}, \frac{3}{2}^-$, and $\frac{5}{2}$ by a confidence level of $10^{-4}$ or better but $\frac{3}{2}^+$ and $\frac{5}{2}^-$ are not rejected. In the region $|\hat{\boldsymbol{\pi}}_{\text{in}}^- \cdot \hat{\mathbf{K}}_{\text{out}}^+| < 0.5$, we again find $\frac{3}{2}^-$ and $\frac{5}{2}^+$ rejected. Moreover $\frac{3}{2}^+$ is favored over $\frac{5}{2}^-$ by a confidence level ratio of 10. From these two samples we conclude $J^P = \frac{3}{2}^+$ is in agreement with the data.

In table 9 we tabulate the moments for $\Sigma(1385)^0$ based on 246 events having $\Lambda\pi^0$ mass between 1360 and 1440 MeV. We note that $t_2^0$ is the only non-zero moment with even-$L$ and all odd-$L$ moments are consistent with zero. As in the case of $\Lambda(1405)$, this state appears to be produced unpolarized. In table 10 we give chi-squared confidence levels for the $\Sigma(1385)^0$ spin-parity analysis. One concludes only that $J = \frac{1}{2}$ is rejected.

Table 7
Spin-parity moments for $\Sigma(1385)^-$

| $J$ | $t_L^M$ | Re $t_L^M$ | $\delta$(Re $t_L^M$) | Im $t_L^M$ | $\delta$(Im $t_L^M$) |
|---|---|---|---|---|---|
| $\frac{1}{2}$ | $t_1^0$ | 0.36 | 0.11 | | |
| $\frac{3}{2}$ | $t_1^0$ | 0.82 | 0.24 | | |
| | $t_2^{-2}$ | − 0.12 | 0.03 | − 0.03 | 0.03 |
| | $t_2^0$ | 0.02 | 0.04 | | |
| | $t_3^{-2}$ | − 0.03 | 0.06 | 0.03 | 0.06 |
| | $t_3^0$ | − 0.13 | 0.08 | | |
| $\frac{5}{2}$ | $t_1^0$ | 1.26 | 0.37 | | |
| | $t_2^{-2}$ | − 0.11 | 0.03 | − 0.17 | 0.07 |
| | $t_2^0$ | 0.02 | 0.04 | | |
| | $t_3^{-2}$ | − 0.05 | 0.11 | 0.06 | 0.11 |
| | $t_3^0$ | − 0.23 | 0.14 | | |
| | $t_4^{-4}$ | − 0.06 | 0.03 | − 0.02 | 0.03 |
| | $t_4^{-2}$ | − 0.04 | 0.03 | − 0.06 | 0.03 |
| | $t_4^0$ | − 0.09 | 0.05 | | |
| | $t_5^{-4}$ | 0.00 | 0.05 | 0.03 | 0.05 |
| | $t_5^{-2}$ | 0.06 | 0.05 | 0.02 | 0.05 |
| | $t_5^0$ | − 0.08 | 0.07 | | |
| $\frac{1}{2}$ | $\gamma t_1^0$ | 0.40 | 0.08 | | |
| $\frac{3}{2}$ | $\gamma t_1^0$ | 0.44 | 0.09 | | |
| | $\gamma t_3^{-2}$ | − 0.03 | 0.06 | 0.10 | 0.06 |
| | $\gamma t_3^0$ | − 0.04 | 0.07 | | |
| $\frac{5}{2}$ | $\gamma t_1^0$ | 0.45 | 0.09 | | |
| | $\gamma t_3^{-2}$ | − 0.03 | 0.06 | 0.10 | 0.06 |
| | $\gamma t_3^0$ | − 0.05 | 0.09 | | |
| | $\gamma t_5^{-4}$ | − 0.06 | 0.05 | 0.04 | 0.05 |
| | $\gamma t_5^{-2}$ | − 0.03 | 0.05 | − 0.01 | 0.05 |
| | $\gamma t_5^0$ | − 0.17 | 0.06 | | |

### *3.2.3. Production characteristics of $\Sigma(1385)^0$*

Although quasi-two-body production at 1.7 GeV/$c$ lacks the peripheral nature exhibited at higher energies, some insight into the production processes can be gained by making use of the simple exchange ($t$-channel) model. We adopt the

Table 8
Results of spin-parity analysis of $\Sigma(1385)^-$

| Selection criteria | Hypothesis | Degrees of freedom | $\chi^2$ | $P(\chi^2)$ |
|---|---|---|---|---|
| Total sample | $J = \frac{1}{2}$(even $L$) | 8 | 40.1 | $< 10^{-5}$ |
| (553 events) | $J^P = \frac{3}{2}^+$ | 4 | 3.3 | 0.50 |
| | $J^P = \frac{3}{2}^-$ | 4 | 32.5 | $< 10^{-5}$ |
| | $J^P = \frac{5}{2}^+$ | 9 | 34.2 | $10^{-4}$ |
| | $J^P = \frac{5}{2}^-$ | 9 | 12.0 | 0.21 |
| $-0.5 < \hat{\pi}_{in} \cdot \hat{K}_{out} < 0.5$ | $J = \frac{1}{2}$(even $L$) | 8 | 13.2 | 0.11 |
| (276 events) | $J^P = \frac{3}{2}^+$ | 4 | 7.8 | 0.10 |
| | $J^P = \frac{3}{2}^-$ | 4 | 29.6 | $< 10^{-5}$ |
| | $J^P = \frac{5}{2}^+$ | 9 | 32.4 | $2 \times 10^{-4}$ |
| | $J^P = \frac{5}{2}^-$ | 9 | 21.9 | 0.008 |

$t$-channel coordinate system defined by Gottfried and Jackson [24]: in the rest frame of the resonance, the $z$ axis is in the production plane and opposite to the direction of the exchanged particle and $y$ is the production normal. The angles $\theta$ and $\phi$ are the usual polar and azimuthal angles of either decay product in this frame. For each reaction there is a choice between meson and baryon exchange and the spin-density-matrix elements provide information on the production processes.

The general form for the decay angular distribution for $\frac{3}{2} \to \frac{1}{2} + 0$ is given by

$$W(\theta, \phi) = \frac{3}{4\pi} [\rho_{33} \sin^2\theta + \rho_{11} (\tfrac{1}{3} + \cos^2\theta) - \frac{2}{\sqrt{3}} \operatorname{Re} \rho_{3-1} \sin^2\theta \cos 2\phi - \frac{2}{\sqrt{3}} \operatorname{Re} \rho_{31} \sin 2\theta \cos\phi] ,$$

subject to the condition $\rho_{33} + \rho_{11} = \frac{1}{2}$. The elements $\rho_{mn}$ are to be determined. The projected $\theta$ and $\phi$ distributions are

$$W(\cos\theta) = \tfrac{1}{4} [(1 + 4\rho_{33}) + (3 - 12\rho_{33}) \cos^2\theta] ,$$

$$W(\phi) = \frac{1}{2\pi} \left[ \left( 1 + \frac{4}{\sqrt{3}} \operatorname{Re} \rho_{3-1} \right) - \frac{8}{\sqrt{3}} \operatorname{Re} \rho_{3-1} \cos^2\phi \right] .$$

The production angular distribution for 236 weighted $\Lambda\pi^0$ events having mass between 1340 and 1430 MeV is shown in fig. 8. Stodolsky and Sakurai [25] have developed a $\rho$-photon model for production of $\frac{3}{2}^+$ states *via* vector meson exchange The model leads to definite predictions for both production and decay angular distributions of the resonance. In particular, the predictions include:

Table 9
Spin-parity moments for $\Sigma(1385)^0$

| $J$ | $t_L^M$ | Re $t_L^M$ | $\delta$(Re $t_L^M$) | Im $t_L^M$ | $\delta$(Im $t_L^M$) |
|---|---|---|---|---|---|
| $\frac{1}{2}$ | $t_1^0$ | 0.31 | 0.19 | | |
| $\frac{3}{2}$ | $t_1^0$ | 0.68 | 0.42 | | |
| | $t_2^{-2}$ | 0.04 | 0.04 | − 0.07 | 0.04 |
| | $t_2^0$ | − 0.32 | 0.06 | | |
| | $t_3^{-2}$ | 0.07 | 0.09 | 0.07 | 0.09 |
| | $t_3^0$ | − 0.12 | 0.13 | | |
| $\frac{5}{2}$ | $t_1^0$ | 1.04 | 0.65 | | |
| | $t_2^{-2}$ | 0.04 | 0.04 | − 0.07 | 0.04 |
| | $t_2^0$ | − 0.30 | 0.06 | | |
| | $t_3^{-2}$ | 0.13 | 0.17 | 0.13 | 0.16 |
| | $t_3^0$ | − 0.21 | 0.24 | | |
| | $t_4^{-4}$ | 0.07 | 0.04 | − 0.04 | 0.04 |
| | $t_4^{-2}$ | − 0.04 | 0.05 | 0.06 | 0.05 |
| | $t_4^0$ | 0.02 | 0.08 | | |
| | $t_5^{-4}$ | − 0.04 | 0.07 | − 0.07 | 0.07 |
| | $t_5^{-2}$ | − 0.09 | 0.08 | 0.11 | 0.08 |
| | $t_5^0$ | − 0.12 | 0.13 | | |
| | $\gamma t_1^0$ | − 0.10 | 0.11 | | |
| $\frac{3}{2}$ | $\gamma t_1^0$ | − 0.11 | 0.12 | | |
| | $\gamma t_3^{-2}$ | − 0.03 | 0.07 | 0.02 | 0.07 |
| | $\gamma t_3^0$ | − 0.02 | 0.08 | | |
| $\frac{5}{2}$ | $\gamma t_1^0$ | − 0.11 | 0.13 | | |
| | $\gamma t_3^{-2}$ | − 0.03 | 0.09 | − 0.03 | 0.09 |
| | $\gamma t_3^0$ | 0.08 | 0.14 | | |
| | $\gamma t_5^{-4}$ | − 0.08 | 0.07 | 0.07 | 0.07 |
| | $\gamma t_5^{-2}$ | 0.00 | 0.07 | 0.09 | 0.07 |
| | $\gamma t_5^0$ | − 0.07 | 0.10 | | |

(a) $\frac{d\sigma}{d\Omega} \propto (F(t)^2 \sin^2\theta)/(t - m^{*2})^2$

where $t$ is the four-momentum transfer squared, $F(t)$ is a slowly varying function, and $m^*$ is the mass of the exchanged particle.

Table 10
Results of spin-parity analysis of $\Sigma(1385)^0$

| Hypothesis | Degrees of freedom | $\chi^2$ | $P(\chi^2)$ |
|---|---|---|---|
| $J = \frac{1}{2}$ | 8 | 40 | $< 10^{-5}$ |
| $J^P = \frac{3}{2}^+$ | 4 | 5.5 | 0.24 |
| $J^P = \frac{3}{2}^-$ | 4 | 2.2 | 0.70 |
| $J^P = \frac{5}{2}^+$ | 9 | 6.9 | 0.66 |
| $J^P = \frac{5}{2}^-$ | 9 | 13.6 | 0.14 |

(b) The $|J, J_y\rangle = |\frac{3}{2}, \pm\frac{3}{2}\rangle$ spin states projected on to the y-axis (production normal) will not be occupied. This leads directly to a decay angular distribution of the form $1 + 3\sin^2\theta\sin^2\phi$ and the corresponding requirements $\rho_{33} = \frac{3}{8}$, Re $\rho_{3-1} = 0.216$; Re $\rho_{31} = 0$ if an Ml transition dominates.

In fig. 8 we show (smooth curve) the normalized production distribution of (a) with $F(t)$ constant and $m^* = 890$ MeV. The confidence level for the fit is 15%. The data are slightly less peripheral than predicted; this effect was also noted by Foreman [26] in $\pi^+ p \to \Sigma(1385)^+ + K^+$ at 1.7 GeV/c. The data of Dahl et al. [1], in $\pi^- p \to \Sigma(1385)^0 K^0$ in the momentum range 1.8–2.2 GeV/c, are inconsistent with this model in that the production angular distribution peaks in the foreward direction. However, the experiment has significant $K^*(890)$ production.

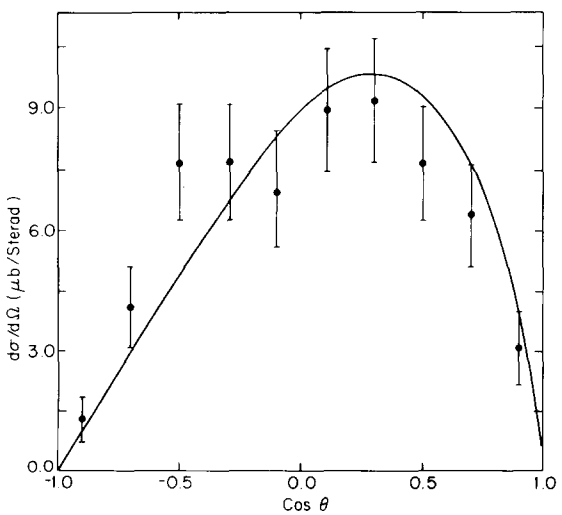


Fig. 8. Differential cross section for $\pi^- p \to \Sigma(1385)^0 K^0$.

Table 11a
t-channel density matrix elements for $\Sigma(1385)^0$

| $\cos\theta_{cm}$ | Events | $\rho_{33}$ | Re $\rho_{3-1}$ | Re $\rho_{31}$ |
|---|---|---|---|---|
| Total | 246 | 0.32 ± 0.03 | 0.16 ± 0.03 | 0.05 ± 0.03 |
| 1.0 – 0.5 | 51 | 0.27 ± 0.09 | 0.12 ± 0.08 | – 0.10 ± 0.07 |
| 0.5 – 0.0 | 88 | 0.34 ± 0.05 | 0.16 ± 0.06 | 0.06 ± 0.05 |
| 0.0 – – 0.5 | 71 | 0.37 ± 0.05 | 0.20 ± 0.06 | 0.09 ± 0.05 |
| – 0.5 – – 1.0 | 36 | 0.20 ± 0.10 | 0.10 ± 0.10 | 0.27 ± 0.10 |
| Predicted | | 0.375 | 0.216 | 0 |

Table 11b
t-channel density matrix elements for $\Sigma(1385)^-$

| $\cos\theta_{cm}$ | Events | $\rho_{33}$ | Re $\rho_{3-1}$ | Re $\rho_{31}$ |
|---|---|---|---|---|
| Total | 553 | 0.15 ± 0.02 | 0.05 ± 0.02 | – 0.03 ± 0.02 |
| 1.0 – 0.5 | 106 | 0.07 ± 0.05 | 0.02 ± 0.05 | 0.01 ± 0.06 |
| 0.5 – 0.0 | 128 | 0.20 ± 0.05 | – 0.03 ± 0.05 | – 0.02 ± 0.05 |
| 0.0 – – 0.5 | 139 | 0.21 ± 0.05 | 0.10 ± 0.04 | – 0.02 ± 0.05 |
| – 0.5 – – 1.0 | 180 | 0.12 ± 0.05 | 0.07 ± 0.04 | – 0.06 ± 0.04 |

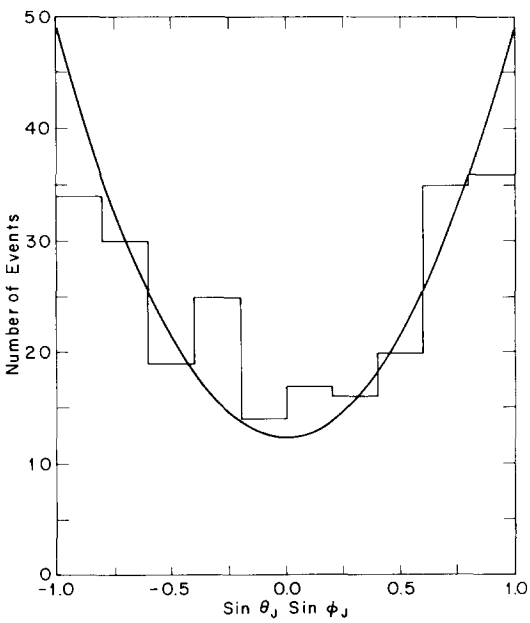


Fig. 9. Distribution of sin $\theta$ sin $\phi$ for the $\Lambda^0\pi^0$ events with mass between 1340 and 1430 MeV.

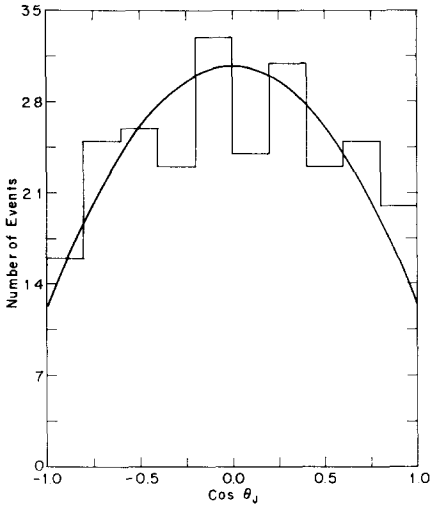


Fig. 10a. Distribution of cos $\theta_J$ for the $\Lambda^0\pi^0$ events with mass between 1340 and 1430 MeV.

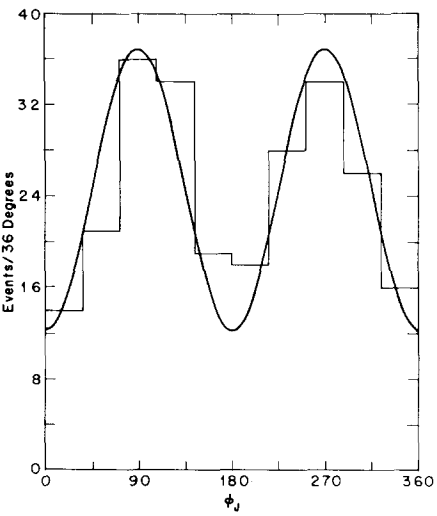


Fig. 10b. Distribution of $\phi_J$ for the $\Lambda^0\pi^0$ events with mass between 1340 and 1430 MeV.

In table 11a we give the $t$-channel density matrix elements for $\Sigma(1385)^0$ along with the prediction of the $\rho$-photon model of Stodoksky-Sakurai. The method of maximum-likelihood was used in the analysis and we give results for four angular ranges as well as the total sample. Agreement with the predictions is slightly better near cos $\theta_{cm} = 0$ where the maximum cross section exists. No background subtraction has been made.

In fig. 9 we show the distribution (total sample) of $\sin\theta \sin\phi$ and compare to prediction (b). The confidence level for the fit is 30%. Figs. 10a, b show the projected $W(\cos\theta)$ and $W(\phi)$ (total sample) along with normalized curves generated from best estimate values of $\rho_{33}$, Re $\rho_{3-1}$ given in table 11a. We conclude the data are in good quantitative agreement with the $\rho$-photon model.

Fig. 11 shows the production angular distribution for 471 weighted $\Lambda\pi^-$ events with mass 1340 to 1430 MeV. Production *via* meson exchange requires the exchanged particle to be doubly charged. Thus, one would expect any simple exchange to be baryon. Indeed, the distribution shows significant backward production. In table 11b, we give the $t$-channel density-matrix elements for $\Sigma(1385)^-$. Again we present results for the total sample and four angular regions. Baryon exchange allows $\rho_{33} \neq 0$ only if $J \geqslant \frac{3}{2}$ is exchanged. Otherwise spin-$\frac{1}{2}$ particles such as $\Sigma$ or $\Lambda$ may be exchanged. The fitted parameters indicate exchange with $J \geqslant \frac{3}{2}$ in the region $-0.5 \leqslant \cos\theta_{cm} \leqslant 0.5$, whereas in the forward and backward regions $J > \frac{1}{2}$ is not required. We speculate the differences between $\Sigma^- K^+$ production (sect. 5), and that of $\Sigma(1385)^- K^+$ production might result from coupling to $J_z = \frac{3}{2}$ This can enhance the production of $\Sigma(1385)^-$ but not of $\Sigma^-$ since the latter cannot be produced, in a simple model, by the exchange of a particle with $J_z = \frac{3}{2}$.

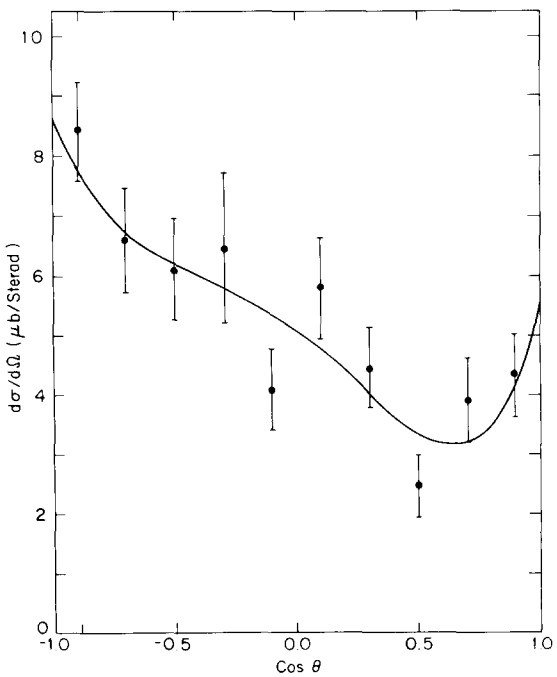


Fig. 11. Differential cross section for $\pi^- p \to \Sigma(1385)^- K^+$.

We have fit the $\Sigma(1385)^-$ production angular distribution to the Legendre polynomial expansion equation (4). The $A_n$ are given in table 5 and the corresponding curve shown in fig. 11. Normalization is such that the cross section for $\Sigma(1385)^-K^+$ is 87% of the cross section for $\Lambda\pi^-K^+$. For completeness we present in table 5 the coefficients $A_n$ for the production of $\Sigma(1385)^oK^o$. Normalization is to 73% of the cross section for $\Lambda\pi^oK^o$.

## 4. Branching fraction of $\Sigma(1385)$ into $\Sigma\pi$

An estimate of the branching ratio

$$R = \frac{\Sigma(1385)^- \to \Sigma\pi}{\Sigma(1385)^- \to \Lambda\pi}$$

can be obtained, in principle, from the final states $\Sigma^o\pi^-K^+$ (172 events), $\Sigma^-\pi^oK^+$ (187 events), and $\Lambda\pi^-K^+$ (722 events). Previous measurements of $R$ [21] give a world average of (11 ± 5)%. Because of this small branching fraction, the $(\Sigma\pi)^-$ data do not exhibit a strong resonant signal in the mass plot of the total sample. However, when a center of mass production angle selection of $\hat{\boldsymbol{\pi}}_{in} \cdot \hat{\mathbf{K}}_{out} \leqslant -0.5$ is made, it is possible to extract $R$ from the data. Unfortunately, this cut reduces the sample to 215 events $\Lambda\pi^-$ and 116 events $(\Sigma\pi)^-$ invariant mass distributions were each fit to an incoherent mixture of phase space background and p-wave Breit-Wigner function. The latter had fixed mass (1387 MeV) and width (48 MeV). The amount of $\Sigma(1385)$ was the only parameter to be fit. The calculation of $R$ is given below in table 12.

Table 12
The calculation of $R$

| Final state | $(\Sigma\pi)^-$ | $(\Lambda\pi)^-$ |
|---|---|---|
| Total events | 359 | 722 |
| No. of events for which $\hat{\boldsymbol{\pi}}_{in} \cdot \hat{\mathbf{K}}_{out} \leqslant -0.5$ | 116 | 215 |
| Fraction of total events surviving angle cut | 0.32 | 0.30 |
| Fitted resonance intensity inside angle cut | 0.20 ± 0.11 | 0.96 ± 0.05 |
| Fraction of total events from resonance production inside angle cut | 0.065±0.033 | 0.29 ± 0.02 |
| Total cross section ($\mu$b) | 32.9 ± 2.5 | 76.0 ± 5.5 |
| Cross section for resonance production inside angle cut ($\mu$b) | 2.1 ± 1.2 | 22.1 ± 2.0 |

From the above cross sections we arrive at the value

$$R = \frac{\Sigma\pi}{\Lambda\pi} = \frac{2.1 \pm 1.2}{22.1 \pm 2.0} = 0.10 \pm 0.05$$

which agrees well with the world average. Similarly one obtains the ratio

$$R' = \frac{\Sigma\pi}{\Sigma\pi + \Lambda\pi} = 0.09 \pm 0.04 .$$

## 5. Two-body final states

The reactions

$$\pi^- p \rightarrow \Sigma^- K^+ ,$$
$$\rightarrow \Sigma^o K^o ,$$
$$\rightarrow \Lambda K^o$$

have been studied to determine differential cross sections and $\Lambda^o$ polarization as a function of production angle. These reactions have been analysed extensively in this energy region by Dahl et al. [1] and a complete bibliography has been given by these authors.

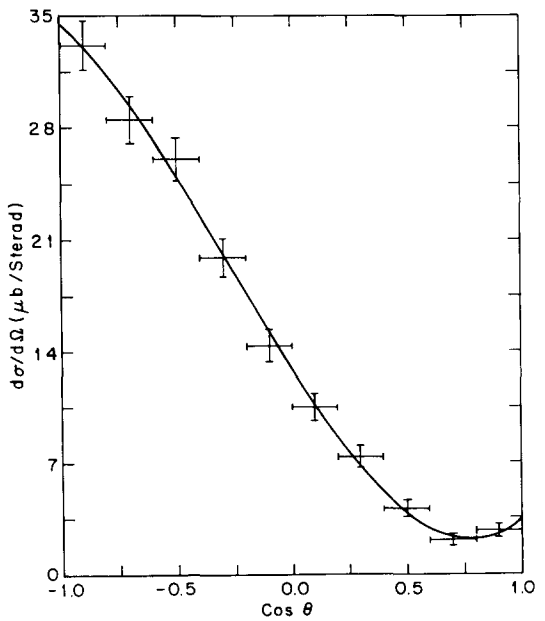


Fig. 12. Differential cross section for $\pi^- p \rightarrow \Sigma^- K^+$.

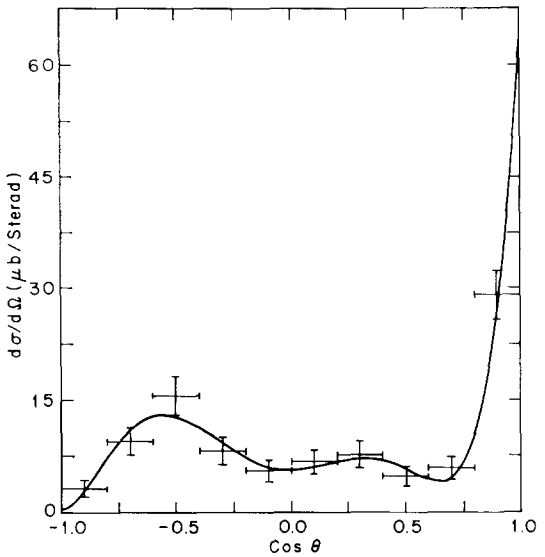


Fig. 13. Differential cross section for $\pi^- p \rightarrow \Sigma^0 K^0$.

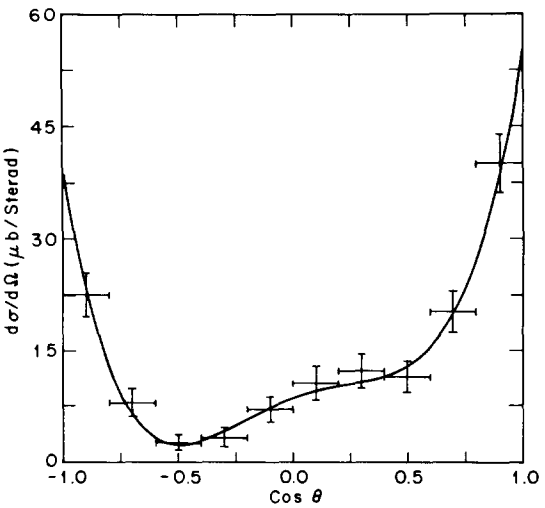


Fig. 14. Differential cross section for $\pi^- p \rightarrow \Lambda^0 K^0$.

The data were selected according to the criteria discussed in subsect. 2.1. and weighted to correct for detection losses. The differential cross sections have been normalized to the total cross sections and are shown in figs. 12–14. The qualitative characteristics of the three production distributions are in agreement with a simple

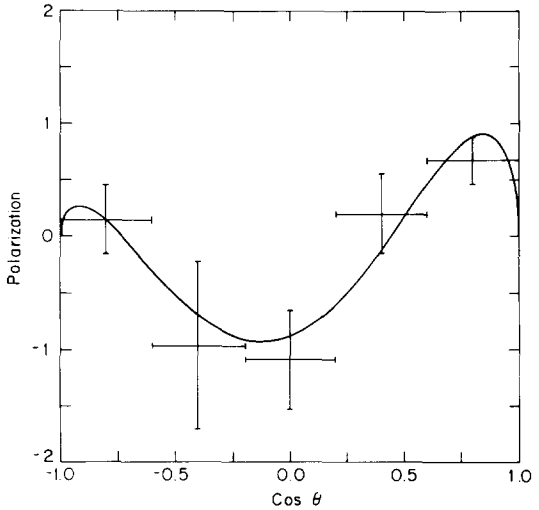


Fig. 15. Λ polarization for $\pi^- p \to \Lambda^0 K^0$.

exchange model in that $\Lambda^0 K^0$ and $\Sigma^0 K^0$ have forward enhancements characteristic of meson exchange while $\Sigma^- K^+$ is sharply peaked in the backward direction.

Each differential cross section has been parameterized by the Legendre polynomial expansion equation (4). The normalization to total cross section is expressed as $A_0 = \sigma_{total}/4\pi$. The fitting was done by the method of least squares and the polynomial was determined by the highst order which gave a significant improvement in the chi-squared confidence level. The coefficients, $A_n$, are summarised in table 5 and the resulting curves appear on figs. 12–14. The polarization of the Λ in the final state $\Lambda^0 K^0$ has been determined in the standard way and has been fitted to the expansion

$$\mathbf{P} = \hat{\mathbf{n}} \sum_n B_n P_n^1(\cos\theta)$$

where $\hat{\mathbf{n}} = (\hat{\boldsymbol{\pi}}_{in} \times \hat{\mathbf{K}}_{out})/|\hat{\boldsymbol{\pi}}_{in} \times \hat{\mathbf{K}}_{out}|$. The coefficients $B_n$ are also given in table 5 and the resulting curve is shown in fig. 15.

The authors wish to acknowledge the efforts of their scanning and measuring staff and of Mrs. A. Maxwell. Numerous discussions with Professor J. Ashkin were most helpful. Drs. F. Di Bianca, R. Endorf and C. Meltzer contributed to many phases of the experiment. Professor J.B. Shafer provided us with some of the programs used in the spin-parity analyses. R.W.K. would like to thank Drs. T.G. Walker and G. Manning for their hospitality during a sabbatical year at the Rutherford Laboratory where some of this work was completed.

## References


[1] O.I. Dahl, L.M. Hardy, R.I. Hess, J. Kirz and D.H. Miller, Phys. Rev. 163 (1967) 1377; O.I. Dahl, L.M. Hardy, R.I. Hess, J. Kirz, D.H. Miller and J.A. Schwartz, Phys. Rev. 163 (1967) 1430.
[2] N. Byers and S. Fenster, Phys. Rev. Letters 11 (1963) 52.
[3] R.H. Dalitz, T.C. Wong and G. Rajasekaran, Phys. Rev. 153 (1967) 1617.
[4] A. Engler, H.E. Fisk, R.W. Kraemer, C.M. Meltzer, J.B. Westgard, T.C. Bacon, D.G. Hill, H.W.K. Hopkins, D.K. Robinson and E.O. Salant, Phys. Rev. Letters 15 (1965) 224.
[5] T.J. Devlin, J. Solomon and G. Bertsch, Phys. Rev. Letters 14 (1965) 1031.
[6] D.W. Thomas, Ph. D. Thesis, Carnegie-Mellon University (1971).
[7] R. Dalitz and S.F. Tuan, Ann. of Phys. 10 (1960) 307.
[8] R. Dalitz, High energy physics, eds. C. de Witt and M. Jacob (Gordon and Breach, New York, 1965) 251.
[9] R. Dalitz, Invited paper presented to the Hyperon Resonances Conference, Duke University, April 1970.
[10] G. Ebel, A. Mullensiefen, H. Pilkuhn, F. Steiner, D. Wegener, M. Gourdin, C. Michael, J.L. Petersen, M. Roos, B.R. Martin, G. Oades and J.J. De Swart, Nucl. Phys. B33 (1971) 317.
[11] K.O. Bunnell, D. Cline, R. Laumann, J. Mapp and J.L. Uretsky, Nuovo Cimento Letters 3 (1970) 224.
[12] D. Cline, R. Laumann and J. Mapp, Phys. Rev. Letters 26 (1971) 1194.
[13] J. Kim, Phys. Rev. Letters 19 (1967) 1074.
[14] K.M. Watson, Phys. Rev. 88 (1952) 1163.
[15] M.H. Ross and G.L. Shaw, Ann. of Phys. 13 (1961) 147.
[16] Y.A. Chao, R.W. Kraemer, B.R. Martin and D.W. Thomas, Nucl. Phys. B56 (1973) 46.
[17] J. Thompson, Proc. Duke Conf. on hyperon resonances, ed. E.C. Fowler.
[18] D. Bereley, P. Yamin, R. Kofler, A. Mann, G. Meisner, S. Yamamoto, J. Thompson and W. Willis, Phys. Rev. D1 (1970) 1969.
[19] B.R. Martin and M. Sakitt, Phys. Rev. 183 (1969) 1345.
[20] A.D. Martin and G.G. Ross, Nucl. Phys. B16 (1970) 479.
[21] Particle Data Group, Phys. Letters 39B (1972) 1.
[22] W.S.C. Williams, An introduction to elementary particles (Academic Press, New York, 1971) 285;
D.B. Lichtenberg, Unitary symmetry and elementary particles, (Academic Press, New York, 1970) 217.
[23] J.B. Shafer and D.O. Huwe, Phys. Rev. 134 (1964) B1372.
[24] K. Gottfried and J.D. Jackson, Nuovo Cimento 33 (1964) 3589.
[25] L. Stodolsky and J.J. Sakurai, Phys. Rev. Letters 11 (1963) 90;
L. Stodolsky, Phys. Rev. 134 (1964) B1099.
[26] F.L. Foreman, Thesis, University of Pennsylvania (1969).